Article

Rapid Estimation of Sulfur Content in High-Ash Indian Coal Using Mid-Infrared FTIR Data

Anubhav Shukla [1,2], Anup K. Prasad [1,*], Sameeksha Mishra [1], Arya Vinod [1] and Atul K. Varma [2]

[1] Photogeology and Image Processing Laboratory, Department of Applied Geology, Indian Institute of Technology, Indian School of Mines, Dhanbad 826004, India; jrf.17dr000435@agl.iitism.ac.in (A.S.); sameeksha.19dr0131@agl.iitism.ac.in (S.M.); 21dr0034@agl.iitism.ac.in (A.V.)

[2] Coal Geology and Organic Petrology Laboratory, Department of Applied Geology, Indian Institute of Technology, Indian School of Mines, Dhanbad 826004, India; atul@iitism.ac.in

[*] Correspondence: anup@iitism.ac.in

Abstract: High-ash Indian coals are primarily used as thermal coal in power plants and industries. Due to the presence of sulfur in thermal coal, flue gas is a major environmental concern. Conventional methods (Ultimate Analysis of Coal) for sulfur content estimation are time-consuming, relatively costly, and destructive. In this study, Fourier-transform infrared (FTIR) spectroscopy has emerged as a promising alternative method for the rapid and nondestructive analysis of the sulfur content in coal. In the present study, the actual sulfur content in the coal samples was determined using Ultimate Analysis (CHNS analyzer). In contrast, mid-infrared FTIR spectroscopic data (4000–400 cm^{-1}) were used to analyze the functional groups related to sulfur or its compounds in the coal samples to predict the sulfur content. A comparison of sulfur estimated using a CHNS analyzer and predicted using mid-infrared spectroscopy (FTIR) data shows that it can accurately predict sulfur content in high-ash Indian coals using the piecewise linear regression method (Quasi-Newton, QN). The proposed FTIR-based sulfur prediction model showed a coefficient of determination (R^2) of up to 0.93, where the total no. of samples (Coal + KBr pellets, n) was 126 (using 17:1 split, K-fold cross validation). The root-mean-square error (RMSE, wt.%) is 0.0035, mean bias error (MBE, wt.%) is -0.0003, MBE (%) is 3.31% and mean absolute error (MAE, wt.%) is 0.0020. The two-tailed t-test and F-test for mean and variance indicated no significant difference between the pair of values of observed sulfur (S_{CHNS}, wt.%) using CHNS data and the model predicted sulfur (S_{FTIR}, wt.%) using FTIR data. The prediction model using mid-infrared FTIR spectroscopy data and the Quasi-Newton method with a breakpoint and loss function performs well for coal samples from the Johilla Coalfield, Umaria. Thus, it can be a valuable tool for analyzing sulfur in other ash-rich coals from various basins worldwide.

Keywords: sulfur content; Fourier-transform infrared spectroscopy (FTIR); Quasi-Newton (QN) method; high ash; Indian coal

1. Introduction

Coal is a mixture of heterogeneous materials composed of organic and inorganic substances [1–3]. Sulfur in coal is present in organic and inorganic forms [4]. It is an important parameter for determining the suitability for various applications, such as power generation and steel production. It can negatively affect the environment, climate, and industrial processes. Organic sulfur in coal refers to sulfur that is chemically bonded to the organic matter in coal. It can be difficult to remove it from coal during processing, and it can also contribute to air pollution when coal is burned. Inorganic sulfur refers to sulfur that is not chemically bonded to the organic matter in coal. It can occur in various forms, such as sulfates, sulfides, and elemental sulfur. It is typically found to be less harmful to the environment while burning. Pyrite is the primary inorganic sulfur impurity in the majority of coals [4–6].

Sulfur dioxide (SO_2) emissions primarily come from burning fossil fuels, such as coal, oil, and industrial processes involving sulfur-containing materials. The majority of SO_2 in the atmosphere is the result of human activity, specifically emissions from coal-fired thermal power plants, where practically all sulfur in coal is oxidized to SO_2 during combustion [7]. Improper coal combustion produces a range of pollutants, including sulfur dioxide (SO_2), nitrogen oxides (NOx), particulate matter, and carbon dioxide (CO_2). Various technologies have been developed to remove or reduce the amount of sulfur dioxide emitted during combustion [8]. One common approach is to use flue gas desulfurization (FGD) systems, which can remove up to 95% of SO_2 emissions from a power plant. FGD systems typically use a variety of methods, such as wet scrubbing with a calcium-based reagent or dry sorbent injection, to capture and remove sulfur dioxide from flue gas [9,10]. Thus, rapid estimation of the sulfur content in coal used in thermal power plants is essential for operational (removal processes) and environmental aspects.

In addition to FGD systems, switching to alternative fuels and improving the efficiency of combustion processes can reduce the emission of toxicants from coal-fired thermal power plants [11,12]. The chemical nature of aerosols is critical for understanding their overall input to the atmosphere and related climate change issues. Carbonaceous aerosols are highly absorbing in nature, whereas sulfate aerosols are usually highly scattering in nature. This impacts the atmospheric temperature, cloud processing (seeding and modifying), and climate [13]. Thus, estimation of the sulfur content in coal is important because these emissions lead to acid rain, which can harm crops, forests, and bodies of water and contribute to respiratory problems in humans [14]. Long-term exposure to sulfur oxides (SOx), particularly SO_2 released by coal-fired power plants, can increase the risk of developing cardiovascular disease (CVD) and ischemic heart disease (IHD) [15,16].

Apart from health-related impacts, sulfur can decrease the quality of coke, which is used to produce iron and steel in industrial processes. This can lead to increased costs and lower efficiency in the production process. High-ash thermal coal is considered a lower quality fuel than other types of coal but is still widely used in power plants worldwide due to its low cost and availability. However, the high ash content of coal can pose several challenges to power plant operators, and the foremost challenge is ash accumulation on boiler surfaces. The leftover ash can stick to boiler tubes and other components, reducing their efficiency and increasing the risk of equipment failure [17].

The sulfur content in coal can vary significantly depending on the type and origin of the coal. Knowing the sulfur content of coal allows for the appropriate management and use of the resource and can help ensure compliance with environmental regulations. Many countries have implemented regulations and standards to limit the amount of sulfur emitted from power plants and encourage the use of cleaner and more efficient technologies. For instance, the limits for thermal power plants in India are already specified in the Environment (Protection) Amendment Rules, 2015 [18]. Here are some approximate ranges of sulfur content in coal seams from major coal-producing countries: China is the world's largest producer and consumer of coal [19], and the sulfur content of its coal can vary widely, from less than 0.2% to more than 5%, with an average of approximately 1.5% [20–22]. In the United States, it ranges from less than 0.2% to more than 5%, depending on the region and type of coal [23]. Coal from the Appalachian region tends to have a higher sulfur content [24], whereas coal from the Powder River Basin in Wyoming has a relatively low sulfur content. The sulfur content in Russian coals can vary widely, with some coals containing less than 0.5% sulfur and others containing up to 5% sulfur or more [25]. Coal from the Bowen Basin in Queensland tends to have low sulfur content, whereas coal from the Hunter Valley in New South Wales can have sulfur contents ranging from 0.5% to 1.5% [26]. Indonesian coal is known for its relatively low sulfur content, with typical sulfur levels of less than 1%. In the European Union's coal, sulfur content range from approximately 0.5% to 3% in Germany, Poland, Spain, and the United Kingdom [27].

In India, SO_2 emissions have been increasing recently due to the country's rapidly growing economy and population [13]. The Indian Government has been implementing

policies to reduce SO$_2$ emissions, such as stricter emission standards for vehicles and industries, as well as promoting renewable energy sources [28]. Therefore, it is important to determine the sulfur content of coal before using it to minimize negative impacts.

The sulfur content of coal can vary greatly depending on the location and type of coal being mined in India. It also depends on the organic source, mineralogy, depositional environment, and tectonics. However, basinwise variation is a more specific way to understand the variation in the sulfur content in coal. Coal from the Eastern flank of India, for example, Damodar and Jharia Basin, generally has moderate sulfur content (e.g., Raniganj coalfield, 1%–2%). The Godavari Basin (e.g., Godavari Valley coalfields, <0.5%) and the Western Coalfields (e.g., Nagpur and Chandrapur coalfields, <0.5%) generally have low sulfur contents. The northeastern states of India, such as Assam and Meghalaya, generally have a higher sulfur content than coal from other regions. Assam's coal has a sulfur content as high as 4%–5%, whereas coal from Meghalaya has as high as 6%–7%. On the other hand, coal from the western and southern regions of India, such as Maharashtra and Andhra Pradesh, tends to have lower a sulfur content, e.g., 0.5%–1% [29].

The traditional method for measuring the sulfur content in coal, such as Ultimate Analysis, is time-consuming. The input samples are also combusted during the estimation process in the CHNS analysis, making the process destructive in nature. Depending upon the type of CHNS analyzer equipment, Elementar's vario MACRO cube's special thermal conductivity detector (TCD) and the sample size (10–20 mg) provide better repeatability. Due to the inherent heterogeneity of coal, Advanced Purge and Trap (APT) technology enables the instrument to measure samples with even uncommon cases and provides the highest precision and accuracy in estimation [30].

To find cheaper, easier, and more efficient approaches, several researchers have successfully implemented a wide variety of advanced techniques all over the world [31]. Previous works tried to formulate a method to quickly predict coal's intrinsic and elemental properties [32,33]. Many assistances and pioneering strategies have been acquainted with meeting the challenge of improving the estimation accuracy. Some of the major methods which were being used for determining the sulfur content of coal are as follows: Pyrolysis–Gas Chromatography [34,35], X-ray absorption near-edge structure spectroscopy (XANES), X-ray photoelectron spectroscopy (XPS) [36], X-ray diffraction (XRD) [37], energy-dispersive X-ray fluorescence (ED-XRF) [38], visible Spectrophotometry (VIS) [39], inductively coupled plasma-atomic emission spectroscopy (ICP-AES) [40], laser-induced breakdown spectroscopy (LIBS) [41–44], thermogravimetric–Fourier-transform infrared spectroscopy (TG–FTIR) [45], and Fourier-transform infrared spectroscopy (FTIR) [46–50]. All these methods have their own advantages and limitations. The choice of method depends on the analysis's specific requirements and available equipment.

In the present study, we devised a series of empirical equations and a mathematical model for the first time. Piecewise nonlinear regression and the Quasi-Newton (QN) method were used to estimate the sulfur content in high-ash Indian coals using the FTIR Spectroscopy data. The primary objectives of this study were as follows:

- The use of nondestructive techniques, such as FTIR, has the potential to be a rapid and effective method for estimating sulfur content in high-ash Indian coals. This technique is based on the principle that sulfur compounds (such as sulfates, sulfides, and thiophenes) in coal absorb infrared radiation at specific wavelengths, which can be used to identify and quantify the presence of sulfur.
- The FTIR method is quick and efficient because it does not require additional time for sample preparation and can be performed onsite in coal mines or power plants. It also has the advantage of being able to detect low levels of sulfur, which is important for compliance with environmental regulations.

The present work is structured as follows: In Section 2, the geological setting of the study area is described. Section 3 provides information on the sample location and selected method. The observed (ultimate) and model-predicted (FTIR) results, discussion on the

prediction model, and its validity are presented in Section 4. Finally, the article concludes in Section 5. The complete procedure is summarized in the flowchart shown in Figure 1.
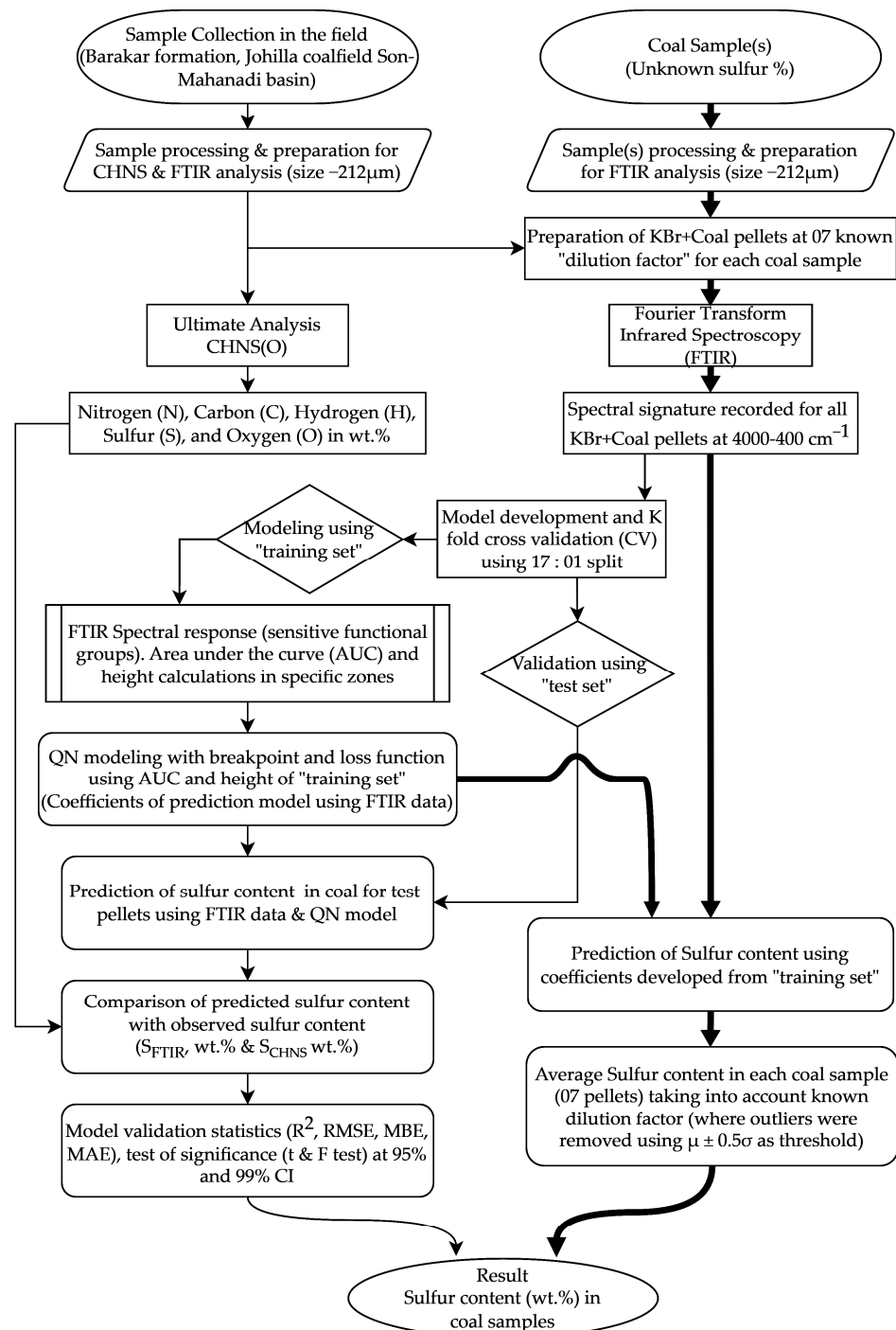

Figure 1. The flowchart summarizes the methodology, techniques, and comparative validation analysis carried out in this study.

2. Geological Setting of the Study Area

Coal deposits are unevenly scattered throughout the world. According to the most recent assessment of global coal reserves, approximately 75% of recoverable reserves are concentrated in five countries: the USA (23.2%), Russian Federation (15.1%), Australia (14%), China (13.3%), and India (10.3%). Global coal production and consumption increased by 5.9% and 6.3% in 2021. In worldwide coal production, India stands 3rd in the row with

13.47 EJ, which increased by 6.9% in 2020. In the worldwide consumption of coal, India ranks 2nd with 20.09 EJ, showing an upsurge of 15.8% in demand compared to the previous year, 2020 (1 Exajoule (EJ) = 40 million tons of hard coal or 95 million tons of lignite and sub-bituminous coal) [51,52].

Indian coal is generally separated into two geological periods, Gondwana Coalfields (~250 million years old) and Tertiary Coalfields (~15–60 million years old) [53]. Gondwana coals contain less moisture and a higher carbon percentage than Tertiary coals and include a significant amount of sulfur and phosphorus. The central-north part of India (Andhra Pradesh, Chhattisgarh, Jharkhand, Madhya Pradesh, Maharashtra, Orissa, Telangana, and West Bengal) represents major Gondwana Coalfields, and the northeastern part (Assam, Arunachal Pradesh, and Meghalaya) have Tertiary Coalfields [29].

The Johilla Coalfield is situated in the Umaria District of Madhya Pradesh, India. This coalfield is positioned on the western flank of the Son Valley Basin and is part of the larger Damodar–Son Coalfield system [54]. The geology of the Johilla Coalfield is characterized by a sequence of sedimentary rocks, including sandstones, shales, and coal seams. These rocks were laid down during the Late Carboniferous to Early Permian period, approximately 300 million years ago. The coal seams in the Johilla Coalfield are inclined, with an average dip of 30–40 degrees [54–56]. They are also faulted and folded, resulting in complex mining conditions. The coal seams in the study area are typically thick and continuous, with an average thickness of approximately 2–3 m. They are primarily composed of sub-bituminous coal and have a high ash content (up to 50%), corresponding to lower-grade coal with a lower heating value than that of bituminous coal [57].

In the Johilla Region, there are two persistent coal seams, the Johilla top and Johilla bottom, which are primarily sub-bituminous to high-volatile bituminous. The organic matter is composed of rich black debris, including biodegraded and structured materials. It mainly consists of land-derived plant fragments and roots at various stages of degradation [57,58]. The high V/I ratio in Johilla coals indicates a high level of maturation. However, the likelihood of oil generation from the source is low due to its high porosity and permeability. Umaria coals have negligible coal bed methane (CBM) potential [59–61].

This area is considered a highly prospective area for coal mining, with estimated reserves of approximately 200 million tons. The coalfield is considered to be a major source of energy for the region, with several large-scale open-pit coal mines and power plants in operation. The coal produced in this coalfield is mainly used for power generation, cement, and metallurgical coke production. The Johilla Coalfield also contains significant reserves of limestone, which is used in cement production, and clay, which is used in the ceramics industry [54–56].

Among Johilla coals, Durain has the highest mineral matter content, whereas Fusain has the lowest. The mineral matter is present in various forms, such as massive impregnation, intimate mixing, deep intergrowth, filling of micropores, and cavity filling. The mineral matters associated with the coal identified under the microscope are pyrite, clays, siderite, and quartz [62–65]. Trace element analysis showed that these coals have low concentrations of W, Sc, Pb, and Be, but notable levels of Y, Ca, and Ni. The highest accumulation of trace elements is found in Barium [66].

The lower Gondwana sandstone in the Johilla coalfield area formed in a highly mixed environment, reflecting a combination of marginal, fluvial, aeolian, and beach conditions [67]. The geomorphology of the area indicates an early stage of maturity, characterized by a dendritic drainage pattern [68,69]. The hilly terrain serves as a source for groundwater recharge [69]. The megaflora and microflora in these beds indicate a transition zone between the upper Karharbari and lower Barakar formations, which suggests that the climate in the Son Valley was cooler than that in the Damodar Basin [70].

The location of the mines/colliery from where respective samples were collected and used in this study is shown over the generalized elevation map of the Umaria District (Figure 2) modified after the groundwater information booklet of the Umaria Dis-

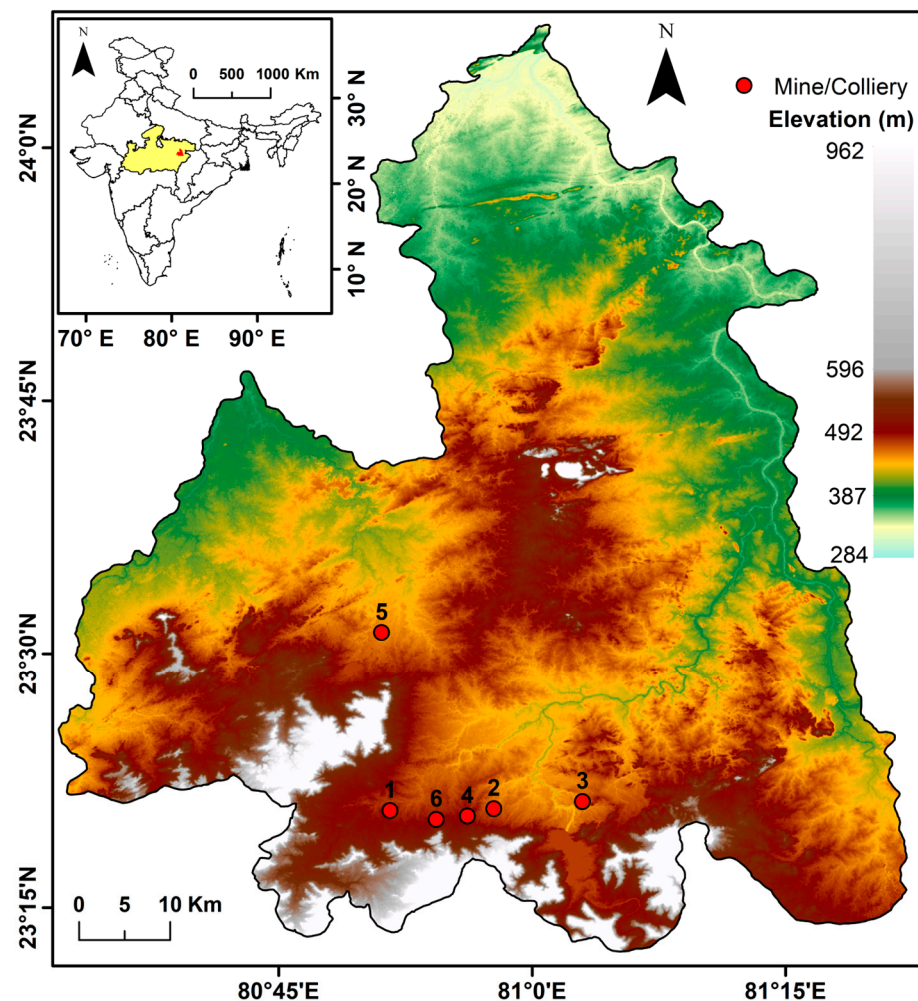trict [71] For a detailed description about the sample location/mine/colliery, please refer to Section 3.1.

Figure 2. Generalized location of the mines over the digital elevation map of Umaria District, Madhya Pradesh, India. Where, 1—Kanchan OCP, 2—Kudri UG; 3—Pali UG; 4—Pinoura UG; 5—Umaria UG; and 6—Vindhya UG.

The stratigraphy of the Umaria Coalfield is represented by Gondwana rocks (Upper Carboniferous to Triassic) consisting of Talchir Formation (Upper Carboniferous to lower Permian) followed by Barakar (lower Permian) and Supra-Barakar Formations [54]. The Supra-Barakar Formation is divided into the Pali-Tiki (upper Permian) and Parsora (Upper Triassic) formations. This is overlain by Chandia Beds (Lower Cretaceous), Lameta beds (Upper Cretaceous), and Deccan trap (Upper Cretaceous to Eocene) formations [55]. Lithologically, the Talchir Formation is characterized by the association of fine- to medium-grained greenish sandstones, shales, and boulder beds (tillite). The Barakar Formation consists of sandstones, shales, and coal seams of the Lower Gondwana sequence from the Lower Permian age [56]. This is the major coal-bearing strata occurring as a triangular-shaped area measuring approximately 15 km^2 in the Johilla Coalfield. The Pali-Tiki Formation comprises coarse-grained sandstone with feldspar grey shale, greenish to mottled clays, carbonaceous shale, and thin coal beds. Variegated shales, clay, and coarse-grained sandstone dominate the Parsora Formations. White clays and medium-grained sandstones depict the Chandia Formations of the Lower Cretaceous. A thin blanket of Lameta beds with greenish sandstones and impure cherty limestones overlapped the Gondwana sediments and was succeeded by basalt flows and dolerite dykes of the Deccan Traps and

recent soil and alluvium [63,68]. The lithostratigraphic succession of the Umaria Area is described in Table 1, respectively.

Table 1. Regional litho-stratigraphic succession near the Johilla Coalfield, Madhya Pradesh, showing the targeted formation (Barakar) for study, marked by **$** modified after [54–56,63,68].

Age	Formation	Lithology
Recent		soil, alluvium
Upper Cretaceous to Eocene	Deccan Trap	basalt flows, dolerite dykes
Upper Cretaceous	Lameta	greenish sandstone, poorly compacted, rarely hard and cherty sandstone, Impure limestone at places cherty, Greenish Mudstone
- - - - - - - - - - - - - - -Unconformity- - - - - - - - - - - - - - -		
Lower Cretaceous	Chandia beds (Jabalpur)	white clay and medium-grained sandstone
Upper Triassic	Parsora	coarse-grained sandstone, mottled clay, and variegated shales
- - - - - - - - - - - - - - -Unconformity- - - - - - - - - - - - - - -		
Upper Permian to Upper Triassic	Pali—Tiki (Supra—Barakars)	coarse-grained sandstone with fresh feldspar grey shale, greenish to mottled clays, carbonaceous shale, and thin coal bands
Lower Permian	Barakar $	(i) coarse- to fine-grained sandstone and shale (ii) coal seams associated with carbonaceous shale (iii) greyish white fine- to medium-grained sandstone with thin carbonaceous shale bands
Upper Carboniferous to Lower Permian	Talchir	(i) fine- to medium-grained sandstone with shale, (ii) green shale to variegated shale, and clay with sandstone (iii) greyish white fine- to medium-grained sandstone with thin carbonaceous shale bands
- - - - - - - - - - - - - - -Unconformity- - - - - - - - - - - - - - -		
Precambrian	Archaean	Archaean gneisses, mica-schist, and metasediments

3. Material and Method

3.1. Sampling

In Table 2, details about the coal sampling sites of the study area are provided, which are also illustrated in Figure 2. For the present study, a total of eighteen (18) coal samples were collected from the 05 underground projects (Kudri UG, Pali UG, Pinoura UG, Umaria UG, and Vindhya UG) and 01 opencast project (Kanchan OCP) of the Johilla Coalfield, Son–Mahanadi Basin, by following the guidelines of ASTM D-2234 [72]. The samples were

crushed and sieved to −212 μm sizes as per the standard methods (ASTM D-4749, [73]) for Ultimate and FTIR analyses.

Table 2. Coal sampling site details of the Johilla Coalfield, Son–Mahanadi Basin, Madhya Pradesh, India.

Sl. No.	Sample	Mine/Locality/Colliery	Seam	Latitude	Longitude	Elevation (in Meters)
1. 2. 3.	JKOB1 JKOL1 JKOL3	Kanchan OCP	JB	23.3451000	80.8600717	443.30
4. 5. 6.	JKUB1 JKUL1 JKUL3	Kudri UG	JB	23.3469217	80.9624067	470.40
7. 8. 9.	JPAB1 JPAL1 JPAL3	Pali UG	JB	23.3538700	81.0498233	466.40
10. 11. 12.	JPIB1 JPIL1 JPIL3	Pinoura UG	L1B	23.3397483	80.9363333	502.40
13. 14. 15.	JUMB1 JUML1 JUML3	Umaria UG	IV	23.5209883	80.8516617	454.10
16. 17. 18.	JVIB1 JVIL1 JVIL3	Vindhya UG	L1B	23.3363750	80.9055150	500.20

Explanation: OCP—opencast project, UG—underground project, JB—Johilla bottom seam, L1B—local seam bottom, IV—seam no. IV.

3.2. Ultimate Analysis

To determine the elemental composition of the coal, the powdered samples were first sieved to obtain a size of −212 μm. Approximately 10 mg of the sample was then wrapped in a tin boat and placed on an automated sample holder of the CHNS analyzer, following the guidelines stated in ASTM D-4239 and D-5373 [74,75]. The Ultimate Analysis was conducted using the Vario Macro Cube of Elementar at the Department of Applied Geology, Indian Institute of Technology (Indian School of Mines) Dhanbad, Jharkhand, India. This benchtop instrument was designed to simultaneously determine the CHNS in samples up to the gram range with high precision and accuracy. During the analysis, the sample was treated at approximately 1150 °C and 850 °C in combustion and reduction tubes, respectively, at a pressure of 1200–1300 mbar in the presence of helium gas purging at a rate of approximately 600 mL/min continuously, and oxygen (O_2) dosing at 50 mL/min for 5 min. The determination of nitrogen (N), carbon (C), and hydrogen (H) was completed in the respective sequence through the process of adsorption and desorption. Finally, sulfur was determined using an infrared detector assembled with the equipment, which can detect even minute levels of sulfur in the sample [30].

3.3. Fourier-Transform Infrared (FTIR) Spectroscopy

FTIR spectroscopy is a widely used nondestructive technique for identifying the functional groups present in coal [76]. The model and make of the FTIR equipment used in this analysis is INVENIO S, BRUKER OPTIK, GmBH (Ettlingen, Germany). In this method, coal samples were typically ground to a fine powder (−212 μm size) and uniformly mixed with KBr powder (IR spectroscopy grade, Uvasol, Kallumbromid, Germany) at a ratio of 1:100. Simultaneously, the FTIR optical bench was flushed with nitrogen gas for 2 h at a rate of approximately 200 L/h before analysis to minimize the effect of moisture and other gases. The prepared mixture of coal and KBr was poured into a hydraulic dye and spread evenly. Later, this dye was placed under a hydraulic press (~6 tons for 5 min) to

make the pellets. The circular thin KBr pellets were inserted into the standard sample holder with a quick-lock base plate. The door of the sample analysis chamber was closed for analysis. The sample pellets were irradiated with infrared radiation, and the resulting absorption spectra were measured and analyzed. The spectra were clipped for the desired frequency range (wavenumber: 4000–400 cm^{-1}). The resultant FTIR data were plotted as an absorbance vs frequency plot (Y-X plot). The absorption spectra of coal samples are typically complex and may contain contributions from other components, such as water, minerals, and organic compounds.

Sample Preparation for Modeling

From 18 coal samples, a total of 126 (07 for each) sample pellets (mix of coal and KBr powder) were prepared at fixed, known concentrations in wt.% (0.10%, 0.20%, 0.30%, 0.40%, 0.60%, 1.00%, and 1.40%) (Figure 3). The spectral response from the Bruker FTIR was recorded individually for 126 sample pellets. Out of 18 coal samples (that is, 126 pellets at fixed coal contents), 119 Coal + KBr pellets were used as the "training set" in the model development, and the coefficients were used to predict the sulfur content in 07 Coal + KBr pellets ("test set") prepared from 01 coal sample using a 17:1 split ("Training set": "test set"; using K-fold cross validation (CV) technique). Thus, the above procedure was repeated 18 times so that 17 coal samples (or 119 pellets) were available for modeling, and 01 independent coal sample (or 07 pellets) was used for validation of the model. Thus, the predicted sulfur values from the "test set" were independent of the "training set" used in the development of the model based on the QN method.
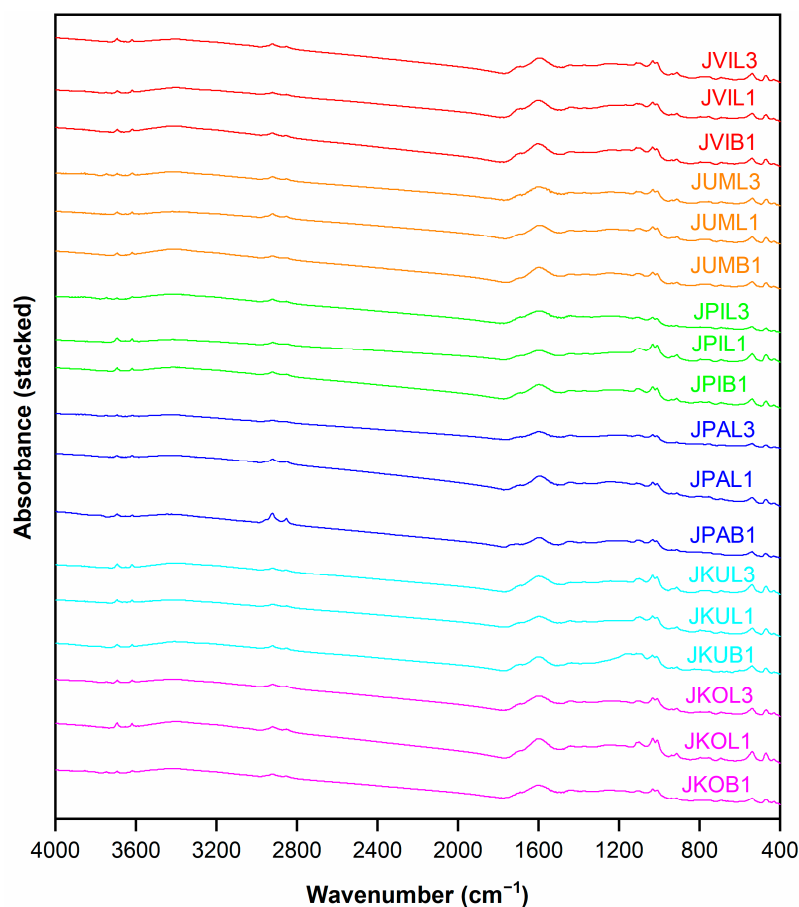

Figure 3. Stacked profile of FTIR spectral signatures recorded in absorbance mode from 18, Coal + KBr pellets. Please see Table 2 to refer to the sample codes and coal sampling sites.

The predicted values (S_{FTIR}, wt.%) of 126 pellets from the FTIR were compared with its known value (S_{CHNS}, wt.%) from CHNS analysis. It is notable that the KBr spectral signature from the FTIR was used as a common reference for baseline correction. The final spectral signature of the 126 pellets from the FTIR was obtained by subtracting the KBr response. The values of the FTIR response from specific zones were computed, and usually the area and height (of peak) in these zones were found to be positive. To avoid negative values after baseline correction, pellets of different contents showing negative values in the area or height were not considered as input parameters for model generation. In the current experiment, 05 pellets FTIR responses were discarded out of 126, due to negative values, which were typically found in the lowest concentration (at 0.10%) of sample (pellets prepared at 0.10% of JKOB1, JKUB1, JKOL3, JKUL3, and JPAL3 samples). Thus, the present study used a total of 121 spectral signatures for modeling.

3.4. Quasi-Newton Method

The Quasi-Newton (QN) method is a generalization of the Newton–Raphson method, a second-order optimization technique that uses the gradient and Hessian matrix of the function to estimate the parameters. It is a numerical optimization technique used to estimate the parameters of a model or function [77]. In estimation problems, the QN method can be used to estimate the parameters of a statistical model by minimizing the sum of squared errors between the observed data and model predictions. This can be performed by iteratively updating the estimates of the parameters and Hessian approximation until the sum of the squared errors reaches a minimum. By approximating the Hessian matrix, the Quasi-Newton method can achieve faster convergence and better performance than the Newton–Raphson method. The Quasi-Newton method can be applied to both experimental data and theoretical models. Theoretically, this method can be used to optimize the model's parameters to match the experimental data [78]. A loss function (Observed–Estimated) was used to minimize the difference between the observed and estimated values.

4. Results and Discussion

4.1. Elemental Composition of Coal

The Ultimate Analysis of Coal provides important information about the quality and suitability of coal for different applications. It is a method of determining the elemental composition of the samples. This method involves the quantitative analysis of the major and minor elements present in coal, i.e., carbon (C), hydrogen (H), nitrogen (N), sulfur (S), and oxygen (O by difference). The results of this analysis are typically expressed as weight percentages of each element present in the sample. The sulfur content in the samples ranges from 0.64 wt.% in JUML3 to 5.72 wt.% in JKUB1. The coal formation process and the depositional environment's effect during coalification justify the higher sulfur content in the coal samples. A detailed account of the Ultimate Analysis of Coal samples is given in Table 3.

Table 3. Elemental composition of coal sample from the Johilla Coalfield.

Mine	Sample	Ultimate Analysis (wt.%)				
		N ^{ad}	C ^{ad}	H ^{ad}	S ^{ad}	O ^{dif}
Kanchan OCP	JKOB1	1.29	65.29	4.15	0.83	28.45
	JKOL1	1.39	63.80	3.84	0.72	30.26
	JKOL3	1.28	62.98	4.04	0.78	30.92
Kudri UG	JKUB1	1.12	53.38	3.54	5.71	36.25
	JKUL1	1.09	61.06	3.84	0.70	33.31
	JKUL3	1.25	60.14	3.66	0.72	34.23
Pali UG	JPAB1	1.32	67.98	3.56	2.19	24.95
	JPAL1	1.28	68.89	3.51	0.96	25.36
	JPAL3	1.23	68.95	3.50	2.19	24.13

Table 3. *Cont.*

Mine	Sample	Ultimate Analysis (wt.%)				
		N ad	C ad	H ad	S ad	O dif
Pinoura UG	JPIB1	1.18	63.92	3.89	1.35	29.66
	JPIL1	1.17	56.42	3.86	1.01	37.54
	JPIL3	1.06	64.10	4.10	0.70	30.04
Umaria UG	JUMB1	1.26	63.83	3.82	0.74	30.35
	JUML1	1.36	64.53	3.77	0.64	29.70
	JUML3	1.29	63.25	3.78	0.62	31.06
Vindhya UG	JVIB1	1.35	59.38	3.61	1.57	34.10
	JVIL1	1.39	59.60	3.53	1.67	33.80
	JVIL3	1.26	63.32	3.53	0.92	30.97
Mean		1.25	62.82	3.75	1.33	30.84
Standard Error		0.02	0.95	0.05	0.28	0.87
Median		1.27	63.56	3.78	0.88	30.64
Mode		1.29	-	3.84	0.72	-
Standard Deviation		0.10	4.04	0.21	1.20	3.68
Sample Variance		0.01	16.35	0.04	1.45	13.56
Minimum		1.06	53.38	3.50	0.62	24.13
Maximum		1.39	68.95	4.15	5.71	37.54

Explanation: N—nitrogen (wt.%), C—carbon (wt.%), H—hydrogen (wt.%), O—oxygen (wt.%), S—sulfur (wt.%), ad—as determined basis, and diff—calculated by difference.

4.2. Identification of Functional Group

In the present study, the identification process of functional groups began with sample preparation. A set of seven (07) pellets were prepared from every sample. In each set of pellets, the amount of KBr was fixed at 220 ± 0.20 mg. The portion of the coal sample ranged approximately between 0.10, 0.20, 0.30, 0.40, 0.60, 1.00, and 1.40 percent. The spectral signatures from each Coal + Kbr pellet were recorded individually. Thus, a total of 126 spectral signatures were recorded; in other words, one signature was recorded for each pellet. This signature also contains the spectra of KBr, which was mixed with the sample. To remove this conglomeration, the spectral signature of only the KBr pellets was recorded and used as a baseline spectrum. The signature recorded from each sample pellet was subtracted from the baseline spectrum, and the resultant spectrum was used for further calculations. The systematic variation in intensity (absorbance) due to known incremental concentration variation can be seen in Figure 4, where the 07 spectral signature of JPAB1, coal + KBr pellet is shown along with the potential peaks sensitive to sulfur.

The FTIR technique utilizes the absorption of infrared radiation. This method can identify and quantify several compounds by analyzing their absorption spectra at specific wavelengths. Organo-petrographic constraints (macerals and degree of coalification), aliphatic bonds, weak bonds, and nonorganic substances within coal are vital in estimating sulfur content. Some of the major sulfur compounds in coal are sulfates, sulfides, and thiophenes. The characteristic absorption peak of sulfoxide (S=O) occured at ~1050 cm^{-1}, an asymmetric stretch of sulfones (S=O) occured at ~1300 cm^{-1}, and a symmetric stretch at ~1150 cm^{-1}. Sulfonates present a strong absorption peak near ~1350 cm^{-1} for asymmetric stretching and near ~1175 cm^{-1} for symmetric stretching. Similarly, in mercaptans (thiols), a stretch of the weak band occurs near ~2550 cm^{-1}. Fourteen (14) peaks were identified and used in the present work. Area and height were calculated for all 14 peaks using the detailed account of peak assignment relating to their functional groups, as defined in Table 4.
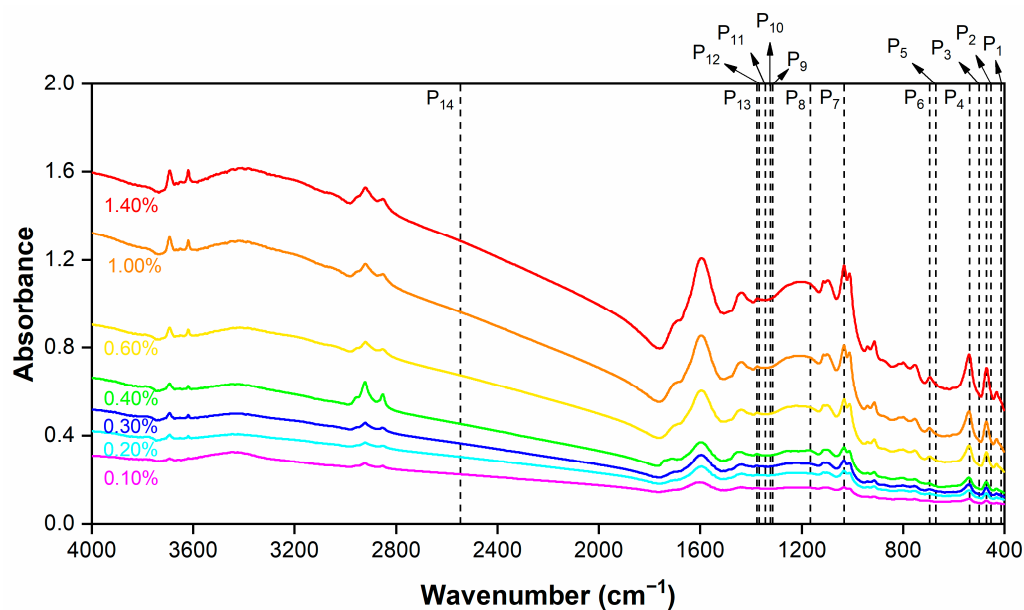
Figure 4. Systematic changes in the level of intensity (absorbance) as observed for Coal + KBr pellets at 07 known concentrations (Seven pellets made at 0.10%, 0.20%, 0.30%, 0.40%, 0.60%, 1.00%, and 1.40% of Coal in Coal + KBr pellets) using FTIR for one of the samples (JPAB1). The location of peaks for sensitive/functional groups related to sulfur in coal is marked as series from $P_1, P_2, \ldots, P_{14}$ (as shown in Table 4).

Table 4. Assigned band details concerning the functional groups of the sulfur compound used in this study, modified after [79,80].

Peak	Wavenumber			Peak Intensity	Functional Groups
	Start	**End**	**Center**		
P_1	442.794	455.650	452.794	w	
P_2	455.650	494.216	469.935	s	S–S stretching
P_3	494.216	505.642	499.931	s	
P_4	505.642	594.201	538.497	w	
P_5	664.192	674.190	671.335	s	C–S stretching
P_6	674.190	718.470	694.189	s	
P_7	1019.856	1064.135	1032.714	s	S=O stretching
P_8	1156.979	1181.261	1165.552	s	SO_2 symmetric stretching
P_9	1306.958	1319.813	1314.103	s	
P_{10}	1319.813	1338.382	1324.101	s	
P_{11}	1338.382	1346.952	1342.670	s	SO_2 asymmetric stretching
P_{12}	1359.808	1374.091	1368.381	s	
P_{13}	1374.091	1385.518	1376.951	s	
P_{14}	2538.213	2553.925	2546.788	w	S–H stretching

Explanation: s—strong, w—weak.

4.3. Model Estimation

A numerical iterative method based on the QN method with a breakpoint was employed to model the nonlinear and linear relationship between the functional groups of sulfur compounds (Table 4) that directly correlate with their content in coal samples. The QN strategy was utilized to limit irregularities and errors in yield estimation and minimize the least square function with the help of a predefined iterative calculation using the piecewise linear regression method.

While considering the breakpoint, the model generates two different variants of the coefficient for the given variables (left and right equations, QN_{bp_L} and QN_{bp_R}) [78]. It is observed that the S% estimated from the left equation (QN_{bp_L} where bp_L = with breakpoint, L = left equation) may provide the closest estimated value compared to the observed experimental value in most of the cases. However, in some cases, out-of-range S% values are estimated by the left equation as compared to the experimental values. Thus, the interquartile range (IQR) was calculated to detect and remove this out of range value(s) (if any) by flagging the values over the maximum and minimum limit, which is $\pm 1.5 \times IQR$, which is calculated using the QN_{bp_L}. Thus, if the estimated value of S% from QN_{bp_L} is out of range, the average S% value was obtained by averaging the S% obtained from the left (QN_{bp_L}) and right (QN_{bp_R}) equations and is denoted as S% from $QN_{bp(avg)}$ (bp = with breakpoint, avg = average). This strategy of using a threshold to detect out-of-range values also helps to minimize the error in estimating the sulfur content in unknown sample(s), thereby improving the efficacy of the FTIR-based estimation of S%.

Using this approach, the resultant values provided the best possible estimate of sulfur content. The resultant S% values are denoted as $QN \approx QN_{bp\_L(con)}$, where (con) represents conditional values. The above-mentioned procedure is summarized by the conditions described below:

Case 1: If the predicted sulfur content (S_{FTIR}, % from QN_{bp_L}) is within the range of A–B (as defined below), then the value from the QN_{bp_L} model is considered as equal to QN.

Case 2: If the predicted sulfur content (S_{FTIR}, % from QN_{bp_L}) is outside the range of A–B), then the value from the $QN_{bp(avg)}$ model is considered as equal to QN.

Where, A = Q1 − (IQR × 1.5); B = Q3 + (IQR × 1.5); $QN_{bp(avg)} = (QN_{bp\_L} + QN_{bp\_R})/2$; QN_{bp_L} = left equation from QN_{bp} model; QN_{bp_R} = right equation from QN_{bp} model

Further, if any modeled S% value is a below zero (or negative) value, then for this specific sample, the estimated modeled S% value was taken as 0.

A detailed statistical analysis was carried out to test the performance of the proposed model using FTIR data employing the spectral response of the functional groups assigned to the sulfur compounds. The measures of central tendency (Mean), measures of dispersion (Standard deviation), measures of systematic error (MBE), measures of the magnitude of error (MAE), and measures of dispersion in residuals (RMSE) were calculated using the standard formulas [81].

The scatter plot with the linear fit (Figure 5) shows the results obtained from the experimental (CHNS) and modeled (FTIR) S%. It showed a relatively high coefficient of determination ($R^2 = 0.93$). Moreover, lower RMSE, MBE, and MAE values and high R^2 indicate a strong linear relationship between the observed sulfur (S_{CHNS}, wt.%) using CHNS data and the model-predicted sulfur (S_{FTIR}, wt.%) using FTIR data. The FTIR method delivers rapid results as compared to traditional Ultimate Analysis.

The boxplot depicts that the sulfur content observed in the coal sample through the traditional methods (using Ultimate Analysis) and the proposed methodology (using FTIR spectroscopy) in this study is significantly equivalent in a range, as shown by the interquartile range and mean. MBE (in wt.%, average = −0.0003), MBE (in %, ≈3.31%), and MAE (0.0020, wt.%) are relatively low, which is visible in the distribution of the mean bias error in Figure 6. MBE, wt.% ranges from approximately −0.010, wt.% to 0.018, wt.%. It was observed that the samples prepared at 0.20%, 0.30%, 0.40%, 0.60%, 1.00%, and 1.40% concentrations provided better results than the ones at 0.10%.
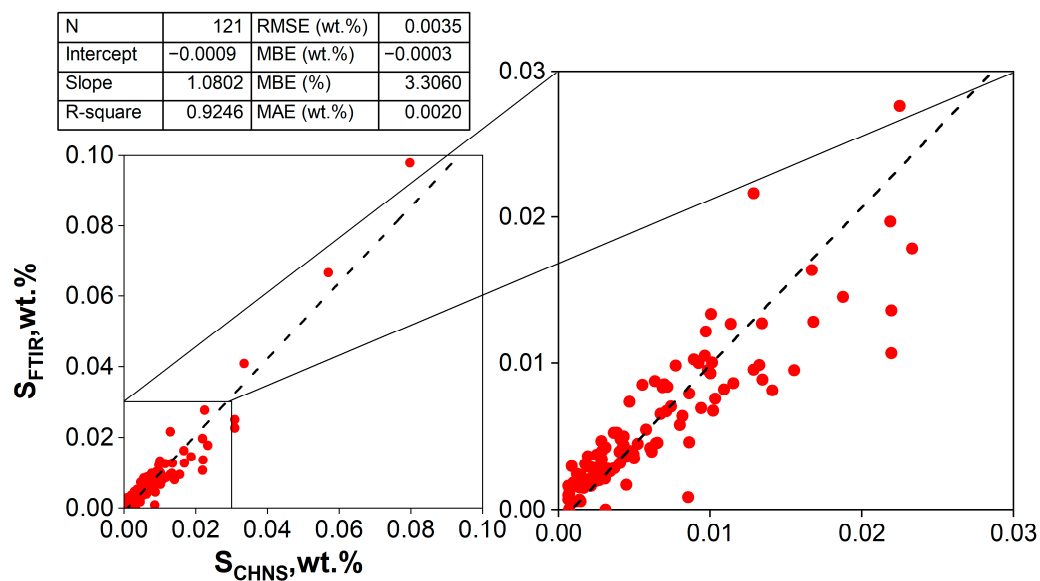
N	121	RMSE (wt.%)	0.0035
Intercept	−0.0009	MBE (wt.%)	−0.0003
Slope	1.0802	MBE (%)	3.3060
R-square	0.9246	MAE (wt.%)	0.0020

Figure 5. The scatter plot shows the correlation between the observed sulfur (S_{CHNS}, wt.%) using CHNS data and the model-predicted sulfur (S_{FTIR}, wt.%) using FTIR data with the measures of error RMSE (%) = 36.36%; MBE (%) = 3.31%; and $R^2 \approx 0.93$. Where S_{CHNS}–observed sulfur using CHNS data; S_{FTIR}—model-predicted sulfur using FTIR data; N—no. of data points; R^2—coefficient of determination; RMSE—root mean square error; MBE—mean bias error; and MAE—mean absolute error.
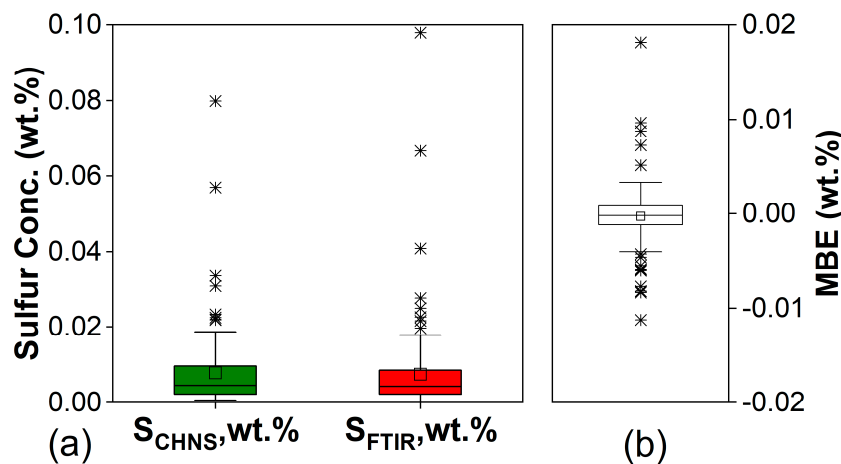
Figure 6. (**a**) Comparison between the variation in observed sulfur (S_{CHNS}, wt.%) using CHNS data and the model-predicted sulfur (S_{FTIR}, wt.%) using FTIR data. (**b**) distribution of mean bias error in wt.%.

A two-tail paired t-test for mean ($\bar{x}$) was conducted at 95% CL and $\alpha = 0.05$, and 99% CL and $\alpha = 0.01$, to examine if there was a significant difference between the means (μ_d) of S (in %) obtained from the two groups (that is, between the observed (SCHNS, wt.%) and model-predicted (SFTIR, wt.%) S values).

For two-tail paired t-test: Null Hypothesis: H_0: $\mu_d = 0$; and Alternative Hypothesis: H_1: $\mu_d \neq 0$.

From the two-tail paired t-test (Table 5), it is concluded that in the null hypothesis Ho is accepted. Therefore, it is evident that the mean of the observed values (S_{CHNS}, wt.%) is significantly similar to the mean of the model-predicted values (S_{FTIR}, wt.%) at 95% confidence level, where $\alpha = 0.05$ and 99% confidence level, where $\alpha = 0.01$.

Table 5. Results of two-tail paired t-test for comparison of the different means of sulfur content obtained via the model-predicted (S_{FTIR}, wt.%) and observed (S_{CHNS}, wt.%) methods.

Pair	$\bar{x}$	S^2	n	df	95% Confidence Level & α = 0.05				99% Confidence Level & α = 0.01			
					t_{stat}	*p*-Value	$t_{critical}$	H_0: μ_d = 0	t_{stat}	*p*-Value	$t_{critical}$	H_0: μ_d = 0
$S_{FTIR(wt.\%)}$	0.0075	0.0001	121	120	1.0529	0.2945	1.9799	T	1.0529	0.2945	2.6174	T
$S_{CHNS(wt.\%)}$	0.0078	0.0001										

Similarly, a two-tail F-test was conducted for variance (S^2) at 95% CL, where α= 0.05, and 99% CL, where α= 0.01, to examine the significant difference between the observed (S_{CHNS}, wt.%) and modeled-predicted (S_{FTIR}, wt.%) variance.

For two-tail F-test: Null Hypothesis: H_0: $\sigma_o^2 = \sigma_p^2$; and Alternative Hypothesis: H^1: $\sigma_o^2 \neq \sigma_p^2$.

From the two-tail F-test (Table 6), it is concluded that the null hypothesis H_0 is accepted. Thus, it can be inferred that the variance of the observed (S_{CHNS}, wt.%) values (σ_o^2) is significantly similar to the variance of the model-predicted (S_{FTIR}, wt.%) values (σ_p^2), at 95% confidence level, where α = 0.05 as well as the 99% confidence level, where α = 0.01. The acceptance region ($F_{stat} < F_{table}$) for the F-test, at the 95% confidence level, is 0.6980–1.4327, and at 99% confidence level, is 0.6229–1.6055.

Table 6. Results of two-tail F-test for comparison of the difference in the variance of sulfur content obtained via model-predicted (S_{FTIR}, wt.%) and observed (S_{CHNS}, wt.%) methods.

Pair	$\bar{x}$	S^2	n	df	95% Confidence Level & α = 0.05				99% Confidence Level & α = 0.01			
					F_{stat}	*p*-Value	CI	H_0: $\sigma_o^2 = \sigma_p^2$	F_{stat}	*p*-Value	CI	H_0: $\sigma_o^2 = \sigma_p^2$
$S_{FTIR(wt.\%)}$	0.0075	0.0001	121	120	1.2620	0.2040	(0.6980, 1.4327)	T	1.2620	0.2040	(0.6229, 1.6055)	T
$S_{CHNS(wt.\%)}$	0.0078	0.0001										

In Figure 7, the coal sample's observed sulfur content is shown along with its modeled estimated value. It was observed that the model estimate (S_{FTIR}, using FTIR data) accurately predicted the sulfur content in coal as compared to the experimental value (S_{CHNS}), with variations primarily stemming from JKUB1 samples. The high content of sulfur in this sample created a regional high for the other samples. Apart from this, all the modeled values (S_{FTIR}, wt.%) were closer to their observed experimental values (S_{CHNS}, wt.%).
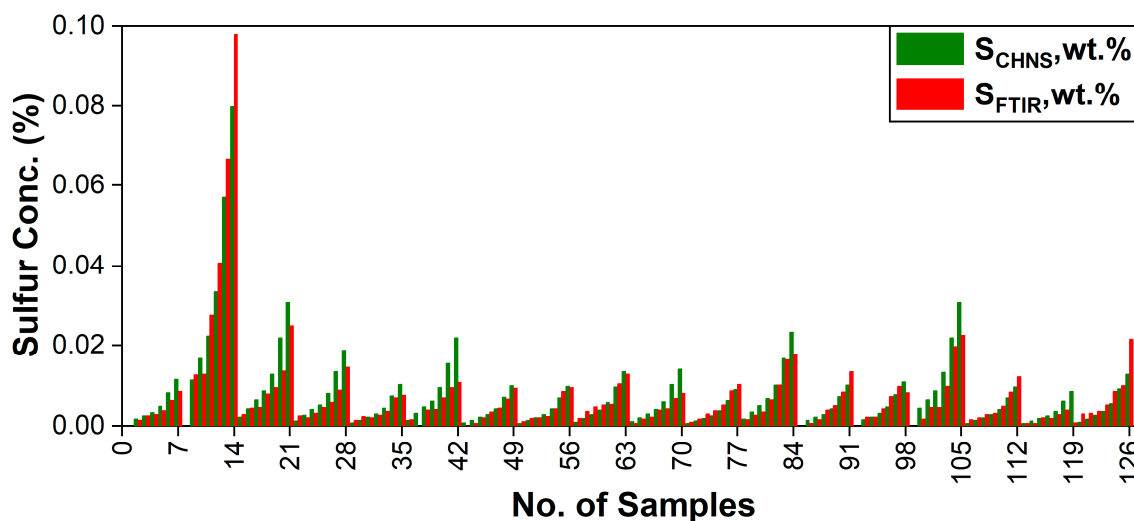

Figure 7. A comparison between the sulfur content (in %) in observed (S_{CHNS}, wt.%) and modeled-predicted (S_{FTIR}, wt.%) coal samples.

4.4. Comparison with Previous Studies

There are several methods used in the previous studies to estimate the sulfur content in coal, namely, laser-induced breakdown spectroscopy (LIBS) with the inclusion of the partial least square regression (PLSR) method, X-ray diffraction (XRD), and visible infrared spectroscopy (VIS) with a convolutional neural network (CNN) (Table 7). Among them, the FTIR data-based model is one of the easiest and most convenient methods for rapidly estimating the sulfur content. This FTIR data-based model provides relatively better results having R^2 = 0.93 and RMSE (wt.%) = 0.0035 as compared to LIBS, XRD, and VIS having R^2 = 0.92; 0.99, and 0.92 and RMSE = 0.898, NA, and 0.053, respectively.

Table 7. Comparison between the methods for estimating sulfur content in coal in previous studies and the present study.

Sl. No.	Reference	Method	Location	Nature and Number of the Samples	R^2	RMSE
1.	[31]	LIBS with PLSR	-	Coal (Blends); N = 60	0.92	0.898
2.	[36]	XRD	Spain	Coal (Sub-bituminous); N = 20	0.99	-
3.	[38]	VIS with CNN	China	Coal; N = 90 Testing + 10 Training	0.92	0.053
4.	This Study	FTIR with QN	India	Coal; N = 121	0.93	0.0035

Explanation, R^2—coefficients of determination, RMSE—root mean square error, LIBS—laser-induced breakdown spectroscopy, PLSR—partial least square regression, XRD—X-ray diffraction, VIS—visible infrared spectroscopy, CNN—convolutional neural network, FTIR—Fourier-transform infrared spectroscopy, and QN—Quasi-Newton method.

5. Summary and Conclusions

In this study, the FTIR data-based model was found to accurately predict the sulfur content in high-ash Indian coals, which is an important characteristic that can affect its combustion properties and environmental impact. According to the proposed FTIR data-based sulfur prediction model, the coefficient of determination (R^2) was ~0.93, based on a sample size (n) of 121. The model had a relatively low RMSE of 0.0035 wt.%, RMSE (%) of 36.36%, and MBE (%) of 3.31%. Furthermore, both the two-tailed t-test and F-test for mean and variance indicated that there was no significant difference between the observed sulfur (S_{CHNS}, wt.%) values and the sulfur predicted by the model (S_{FTIR}, wt.%) using FTIR data. It is notable that the FTIR data-based technique for the determination of sulfur in coal has several advantages as follows:

- Rapid and nondestructive analysis: The FTIR-based model is quick and efficient for estimating the sulfur content, which is useful for quality control and troubleshooting. This allows sample analysis without altering its composition.
- High accuracy and precision: FTIR can provide highly accurate and precise measurements of sulfur content with a relatively low bias.
- Cost effective: FTIR is a relatively low-cost equipment that is easy to use and maintain, making it a popular choice for industrial and laboratory applications. The number and cost of consumables required for analysis are much lower compared to a typical macro CHNSO analyzer.

Considering the variability in other datasets, the model presented in this study can be further improved by using additional data from various basins/coalfields for studies in the future. The RMSE and mean bias (MBE, in %) are expected to reduce further with additional data. The influence of grain size on the spectral response in FTIR and the estimation model needs further investigation. It is recommended that the proposed FTIR data-based model can be potentially applied, with suitable modifications, for determining the sulfur content in other types of natural samples, such as soil, shale, petcoke, etc.

References

1. Teichmüller, M. Organic Petrology of Source Rocks, History and State of the Art. *Org. Geochem.* **1986**, *10*, 581–599. [CrossRef]
2. Taylor, G.H.; Teichmüller, M.; Davis, A.; Diessel, C.F.K.; Littke, R.; Robert, P. *Organic Petrology*; Schweizerbart Science Publishers: Stuttgart, Germany, 1998; Volume XVI, ISBN 978-3-443-01036-2.
3. Suarez-Ruiz, I.; Crelling, J.C. *Applied Coal Petrology: The Role of Petrology in Coal Utilization*; Academic Press: Cambridge, MA, USA, 2008.
4. Calkins, W.H. The Chemical Forms of Sulfur in Coal: A Review. *Fuel* **1994**, *73*, 475–484. [CrossRef]
5. Bodily, D.M.; Wann, J.-P.; Chen, W.; Zhu, X.; Hu, W.; Wadsworth, M.E. Characterization of Mineral and Coal Pyrite. In *1991 International Conference on Coal Science Proceedings, Proceedings of the International Conference on Coal Science, Newcastle upon Tyne, UK, 16–20 September 1991*; Elsevier: Amsterdam, The Netherlands, 1991; pp. 973–976; ISBN 978-0-7506-0387-4.
6. GoldsWorthy, P.; Eyre, D.J.; On, E. Value-in-Use (VIU) Assessment for Thermal and Metallurgical Coal. In *The Coal Handbook: Towards Cleaner Production*; Elsevier: Amsterdam, The Netherlands, 2013; pp. 455–496; ISBN 978-1-78242-116-0.
7. Sulfur Dioxide—DCCEEW. Available online: https://www.dcceew.gov.au/environment/protection/npi/resource/student/sulfur-dioxide-0 (accessed on 16 February 2023).
8. Srivastava, R.K. *Controlling SO_2 Emissions—A Review of Technologies*; DIANE Publishing: Darby, PA, USA, 2000; ISBN 978-1-4289-0157-5.
9. Srivastava, R.K.; Jozewicz, W.; Singer, C. SO_2 Scrubbing Technologies: A Review. *Environ. Prog.* **2001**, *20*, 219–228. [CrossRef]
10. Xu, Y. Improvements in the Operation of SO_2 Scrubbers in China's Coal Power Plants. *Environ. Sci. Technol.* **2011**, *45*, 380–385. [CrossRef]
11. Chakraborty, N.; Mukherjee, I.; Santra, A.K.; Chowdhury, S.; Chakraborty, S.; Bhattacharya, S.; Mitra, A.P.; Sharma, C. Measurement of CO_2, CO, SO_2, and NO Emissions from Coal-Based Thermal Power Plants in India. *Atmos. Environ.* **2008**, *42*, 1073–1082. [CrossRef]
12. Mittal, M.L.; Sharma, C.; Singh, R. Estimates of Emissions from Coal Fired Thermal Power Plants in India. In Proceedings of the 2012 International Emission Inventory Conference, Tampa, FL, USA, 16 August 2012; pp. 13–16.
13. Kuttippurath, J.; Patel, V.K.; Pathak, M.; Singh, A. Improvements in SO_2 Pollution in India: Role of Technology and Environmental Regulations. *Environ. Sci. Pollut. Res.* **2022**, *29*, 78637–78649. [CrossRef] [PubMed]
14. Chou, C.L. Sulfur in Coals: A Review of Geochemistry and Origins. *Int. J. Coal Geol.* **2012**, *100*, 1–13. [CrossRef]
15. Cropper, M.; Gamkhar, S.; Malik, K.; Limonov, A.; Partridge, I. *The Health Effects of Coal Electricity Generation in India*; Resources for the Future: Washington, DC, USA, 2012.
16. Lin, C.-K.; Lin, R.-T.; Chen, P.-C.; Wang, P.; Marcellis-Warin, N.D.; Zigler, C.; Christiani, D.C. A Global Perspective on Sulfur Oxide Controls in Coal-Fired Power Plants and Cardiovascular Disease. *Sci. Rep.* **2018**, *8*, 2611. [CrossRef]
17. Yang, X.; Ingham, D.; Ma, L.; Srinivasan, N.; Pourkashanian, M. Ash Deposition Propensy of Coals/Blends Combustion in Boilers: A Modeling Analysis Based on Multi-Slagging Routes. *Proc. Combust. Inst.* **2017**, *36*, 3341–3350. [CrossRef]
18. CPCB. *The Gazette of India, Extraordinary*; Part-II, Section-3, Sub-Section-II; Government of India: New Delhi, India, 2015.
19. Qian, Y.; Scherer, L.; Tukker, A.; Behrens, P. China's Potential SO_2 Emissions from Coal by 2050. *Energy Policy* **2020**, *147*, 111856. [CrossRef]
20. Hussain, R.; Luo, K. The Geological Availability and Emissions of Sulfur and SO_2 from the Typical Coal of China. *Aerosol Air Qual. Res.* **2019**, *19*, 559–570. [CrossRef]

21. Wei, Q.; Song, W. Mineralogical and Chemical Characteristics of Coal Ashes from Two High-Sulfur Coal-Fired Power Plants in Wuhai, Inner Mongolia, China. *Minerals* **2020**, *10*, 323. [CrossRef]

22. Wu, M.; Shen, J.; Qin, Y.; Qin, Y.; Wang, X.; Zhu, S. Method of Identifying Total Sulfur Content in Coal: Geochemical and Geophysical Logging Data from the Upper Paleozoic in North China. *ACS Omega* **2022**, *7*, 45045–45056. [CrossRef]

23. Allen, T. *U.S. Coal Reserves: An Update by Heat and Sulfur Content*; Energy Information Administration U.S. Department of Energy: Washington, DC, USA, 1993.

24. Trippi, M.H.; Ruppert, L.F.; Attanasi, E.D.; Milici, R.C.; Freeman, P.A. Appalachian Basin Bituminous Coal: Sulfur Content and Potential Sulfur Dioxide Emissions of Coal Mined for Electrical Power Generation. In *Coal and Petroleum Resources in the Appalachian Basin: Distribution, Geologic Framework, and Geochemical Character*; Ruppert, L.F., Ryder, R.T., Eds.; U.S. Geological Survey: Lawrence, KA, USA, 2014; Chapter G.5; p. 68.

25. Małkowski, P.; Tymoshenko, I. The Quality of Coal in Poland, Russia and Ukraine and Its Effect on Dust Emission into the Atmosphere during Combustion. *Tech. Trans.* **2018**, *9*, 141–162. [CrossRef]

26. Hunt, J.W.; Hobday, D.K. Petrographic Composition and Sulphur Content of Coals Associated with Alluvial Fans in the Permian Sydney and Gunnedah Basins, Eastern Australia. In *Sedimentology of Coal and Coal-Bearing Sequences*; John Wiley & Sons: Hoboken, NJ, USA, 1985; pp. 43–60.

27. Atmosphere, Climate & Environment Information Programme. Available online: https://www.lordgrey.org.uk/~f014/usefulresources/aric/Resources/Fact_Sheets/Key_Stage_4/Air_Pollution/27.html (accessed on 28 February 2023).

28. CPCB. *National Ambient Air Quality Status & Trends 2019*; Central Pollution Control Board: New Delhi, India, 2019; pp. 31–37.

29. Central Mine Planning & Design Institute Ltd. *Coal Atlas of India*, 1st ed.; Coal India: Kolkata, India, 1993.

30. Organic Elemental Analyzer Vario MACRO Cube—Elementar. Available online: https://www.elementar.com/en-in/products/organic-elemental-analyzers/vario-macro-cube (accessed on 15 February 2023).

31. Ma, X.M.; Zhang, M.X.; Min, F.F. A Study of Organic Sulfur Analysis in Coal Using Non-Destructive Techniques. *Energy Sources Part Recovery Util. Environ. Eff.* **2015**, *37*, 2716–2723. [CrossRef]

32. Yuan, T.; Wang, Z.; Lui, S.-L.; Fu, Y.; Li, Z.; Liu, J.; Ni, W. Coal Property Analysis Using Laser-Induced Breakdown Spectroscopy. *J. Anal. At. Spectrom.* **2013**, *28*, 1045–1053. [CrossRef]

33. Choi, J.S.; Ryu, C.M.; Choi, J.H.; Moon, S.J. Improving the Analysis of Sulfur Content and Calorific Values of Blended Coals with Data Processing Methods in Laser-Induced Breakdown Spectroscopy. *Appl. Sci.* **2022**, *12*, 12410. [CrossRef]

34. Eglinton, T.I.; Sinninghe Damsté, J.S.; Kohnen, M.E.L.; de Leeuw, J.W. Rapid Estimation of the Organic Sulphur Content of Kerogens, Coals and Asphaltenes by Pyrolysis-Gas Chromatography. *Fuel* **1990**, *69*, 1394–1404. [CrossRef]

35. Xu, X.; McDonald, L.M.; McGowan, C.W.; Glinski, R.J. Examination of Sulfur Forms in Coal by Direct Pyrolysis and Chemiluminescence Detection. *Fuel* **1995**, *74*, 1499–1504. [CrossRef]

36. George, G.N.; Gorbaty, M.L.; Kelemen, S.R.; Sansone, M. Direct Determination and Quantification of Sulfur Forms in Coals from the Argonne Premium Sample Program. *Energy Fuels* **1991**, *5*, 93–97. [CrossRef]

37. Querol, X.; Alastuey, A.; Chinchon, J.S.; Fernandez Turiel, J.L.; Lopez Soler, A. Determination of Pyritic Sulphur and Organic Matter Contents in Spanish Subbituminous Coals by X-Ray Power Diffraction. *Int. J. Coal Geol.* **1993**, *22*, 279–293. [CrossRef]

38. Brown, J.R.; Kasrai, M.; Bancroft, G.M.; Tan, K.H.; Ghen, J.M. Direct Identification of Organic Sulfur Species in Rasa Coal from Sulphur L-Edge X-Ray absorption near-edge spectra. *Fuel* **1992**, *71*, 649–653. [CrossRef]

39. Le, B.T.; Xiao, D.; Mao, Y.; He, D. Coal Analysis Based on Visible-Infrared Spectroscopy and a Deep Neural Network. *Infrared Phys. Technol.* **2018**, *93*, 34–40. [CrossRef]

40. Laban, K.L.; Atkin, B.P. The Direct Determination of the Forms of Sulphur in Coal Using Microwave Digestion Aid i.c.p.-a.e.s. Analysis. *Fuel Energy Abstr.* **2000**, *41*, 137. [CrossRef]

41. Weritz, F.; Ryahi, S.; Schaurich, D.; Taffe, A.; Wilsch, G. Quantitative Determination of Sulfur Content in Concrete with Laser-Induced Breakdown Spectroscopy. *Spectrochim. Acta Part B At. Spectrosc.* **2005**, *60*, 1121–1131. [CrossRef]

42. Gaft, M.; Nagli, L.; Fasaki, I.; Kompitsas, M.; Wilsch, G. Laser-Induced Breakdown Spectroscopy for on-Line Sulfur Analyses of Minerals in Ambient Conditions. *Spectrochim. Acta Part B At. Spectrosc.* **2009**, *64*, 1098–1104. [CrossRef]

43. Qin, H.; Lu, Z.; Yao, S.; Li, Z.; Lu, J. Combining Laser-Induced Breakdown Spectroscopy and Fourier-Transform Infrared Spectroscopy for the Analysis of Coal Properties. *J. Anal. At. Spectrom.* **2019**, *34*, 347–355. [CrossRef]

44. Gazeli, O.; Stefas, D.; Couris, S. Sulfur Detection in Soil by Laser Induced Breakdown Spectroscopy Assisted by Multivariate Analysis. *Materials* **2021**, *14*, 541. [CrossRef]

45. Solomon, P.R.; Serio, M.A.; Carangelo, R.M.; Bassilakis, R.; Gravel, D.; Baillargeon, M.; Baudais, F.; Vail, G. Analysis of the Argonne Premium Coal Samples by Thermogravimetric Fourier Transform Infrared Spectroscopy. *Energy Fuels* **1990**, *4*, 319–333. [CrossRef]

46. Painter, P.C.; Coleman, M.M.; Jenkins, R.G.; Whang, P.W.; Walker, P.L. Fourier Transform Infrared Study of Mineral Matter in Coal. A Novel Method for Quantitative Mineralogical Analysis. *Fuel* **1978**, *57*, 337–344. [CrossRef]

47. Kaihara, M.; Takahashi, T.; Akazawa, T.; Sato, T.; Takahashi, S. Application of near Infrared Spectroscopy to Rapid Analysis of Coals. *Spectrosc. Lett.* **2002**, *35*, 369–376. [CrossRef]

48. Ahmed, M.A.; Blesa, M.J.; Juan, R.; Vandenberghe, R.E. Characterisation of an Egyptian Coal by Mossbauer and FT-IR Spectroscopy. *Fuel* **2003**, *82*, 1825–1829. [CrossRef]

49. Orrego-Ruiz, J.A.; Cabanzo, R.; Mejía-Ospino, E. Study of Colombian Coals Using Photoacoustic Fourier Transform Infrared Spectroscopy. *Int. J. Coal Geol.* **2011**, *85*, 307–310. [CrossRef]

50. Gunavathi, P.; Janaki, D.; Balasubramaniam, P.; Alagesan, A.; Geethanjali, S. Characterization and Identification of Elemental Sulphur, Iron Pyrite, Mineral Gypsum, Phospho Gypsum and Marine Gypsum by Using ATR-FTIR. *J. Pharm. Innov.* **2021**, *10*, 80–86.

51. Dale, S. *BP Statistical Review of World Energy 2022*, 71st ed.; BP: London, UK, 2022; pp. 1–60.

52. Vinay, L.S.; Bhattacharjee, R.M.; Ghosh, N.; Budi, G.; Kumar, J.V.; Kumar, S. Numerical Study of Stability of Coal Pillars under the Influence of Line of Extraction. *Geomat. Nat. Hazards Risk* **2022**, *13*, 1556–1570. [CrossRef]

53. Das, T.; Saikia, B.K.; Baruah, B.P. Formation of Carbon Nano-Balls and Carbon Nano-Tubes from Northeast Indian Tertiary Coal: Value Added Products from Low Grade Coal. *Gondwana Res.* **2016**, *31*, 295–304. [CrossRef]

54. Mukherjee, D.; Ray, S.; Chandra, S.; Pal, S.; Bandyopadhyay, S. Upper Gondwana Succession of the Rewa Basin, India: Understanding the Interrelationship of Lithologic and Stratigraphic Variables. *J. Geol. Soc. India* **2012**, *79*, 563–575. [CrossRef]

55. Dutta, P.K.; Acharyya, S.K.; Jha, N.; Khangar, R.; Khasdeo, L.; Misra, K.G.; Ramanamurty, B.V. Resolving Kamthi-Related Problems in Gondwana Stratigraphy of Peninsular India. *Indian J. Geosci.* **2015**, *69*, 85–102.

56. Ghosh, A.K.; Tewari, R.; Agnihotri, D.; Kar, R.; Pillai, S.S.K.; Bajpai, S.; Tripathi, S.C. *Field Guide Book: Gondwana Formations of South Rewa and Upper Narmada Basins, Central India*; Birbal Sahni Institute of Palaeobotany: Lucknow, India, 2015; p. 40.

57. Singh, K.N.; Singh, R.K.; Katiyar, A. Organic Behavior of Umaria, Korba & IB-Valley Coalfields from SECL & MCL, India. In *Recent Advancements in Mineral and Water Resources*; Excellent Publishers: New Delhi, India, 2016; pp. 43–59.

58. Ram-Awatar; Kumar, M.; Prakash, N. Palynological Analysis of Lower Gondwana Sediments Exposed along the Umrer River South Rewa Basin, Madhya Pradesh, India. *Palaeobotanist* **2005**, *54*, 87–97.

59. Singh, K.N. Role of Vitrinite and Inertinite Ratio in Stratigraphic Correlation and Quality Assessment of Coals—An Example from Johilla and Parts of Korba Coalfields, India. *Minetech* **1991**, *12*, 45–47.

60. Singh, K.N.; Singh, R.P. Source Rock Potential for Hydrocarbon Generation of Johilla Coals, Son Valley, Madhya Pradesh, India. *Indian J. Geol.* **1995**, *67*, 186–190.

61. Singh, K.N. Coal Bed Methane Potentiality—Case Studies from Umaria, Korba and Ib-Valley Coals, Son-Mahanadi Basin. *J. Geol. Soc. India* **2010**, *76*, 33–39. [CrossRef]

62. Singh, R.M.; Singh, M.P.; Singh, K.N.; Dwivedi, C.S. Scanning Electron Micrography of Johillia Coals, Son Valley, M.P. In Proceedings of the National Seminar on Coal Resources of India, Varanasi, India, 27 December 1986; Banaras Hindu University: Varanasi, India, 1987.

63. Singh, R.K.; Singh, K.N.; Navale, G.K.B. The Petrology of Nowrozabad and Birsinghpur Coals, Johilla, M.P., India. In Proceedings of the National Seminar on Coal Resources of India, Varanasi, India, 27 December 1986; Banaras Hindu University: Varanasi, India, 1987; pp. 271–292.

64. Singh, K.N. SEM Analysis of Nowrozabad Coals, Shahdol District, Madhya Pradesh. *Mintech* **1992**, *13*, 54–56.

65. Mishra, V.; Singh, K.N. Microstructural Relation of Macerals with Mineral Matter in Coals from Ib Valley and Umaria, Son-Mahanadi Basin, India. *Int. J. Coal Sci. Technol.* **2017**, *4*, 191–197. [CrossRef]

66. Singh, R.M.; Singh, K.N.; Dwivedi, C.S. Inorganic Constituents of Nowrozabad and Birsinghpur Coals, Johilla Coalfields, Son Valley, M.P. In Proceedings of the National Seminar on Coal Resources of India, Varanasi, India, 27 December 1986; Banaras Hindu University: Varanasi, India, 1987; pp. 183–205.

67. Singh, R.K.; Singh, K.N. The Textural Behaviour of Lower Gondwana Sandstones of Johilla Coalfield Son Valley. *J. Sci. Res.* **1988**, *38*, 87–200.

68. Singh, O.; Singh, K.N. Quantitative Morphometric Analysis of Pali-Parsora Area, Johilla River Basin, Shahdol District, (M.P.). *J. Vikram Univ.* **2000**, *XXVI*, 23–40.

69. Singh, O.; Singh, K.N. Quantitative Morphometric Analysis in Parts of Umarar River Basin, Umaria Area, Madhya Pradesh. *J. Vikram Univ.* **2001**, *XXVII*, 19–26.

70. Gautam, S.; Pillai, S.S.K.; Goswami, S.; Ram-Awatar. Further Contribution to the Mega- and Microfossil Assemblages from the Johilla-Ganjra Nala Confluence, South Rewa Gondwana Basin, Madhya Pradesh, India. *J. Palaeosci.* **2013**, *62*, 199–209. [CrossRef]

71. Ground, C.; Board, W. *District Ground Water Information Booklet, Umaria District, Madhya Pradesh*; Central Ground Water Board North, North Central Region Bhopal: Bhopal, India, 2013.

72. *ASTM D2234/D2234M−17*; Standard Practice for Collection of a Gross Sample of Coal. American Society for Testing and Materials (ASTM): Philadelphia, PA, USA, 2017.

73. *ASTM D4749−12*; Standard Test Method for Performing the Sieve Analysis of Coal and Designating Coal Size. American Society for Testing and Materials (ASTM): Philadelphia, PA, USA, 2012.

74. *ASTM D4239−18*; Standard Test Method for Sulfur in the Analysis Sample of Coal and Coke Using HighTemperature Tube Furnace Combustion. American Society for Testing and Materials (ASTM): Philadelphia, PA, USA, 2018.

75. *ASTM D5373−16*; Standard Test Methods for Determination of Carbon, Hydrogen and Nitrogen in Analysis Samples of Coal and Carbon in Analysis Samples of Coal and Coke. American Society for Testing and Materials (ASTM): Philadelphia, PA, USA, 2016.

76. Othman, N. IR Spectroscopy in Qualitative and Quantitative Analysis. In *Infrared Spectroscopy-Perspectives and Applications*; IntechOpen: Rijeka, Croatia, 2022.

77. Singh, R.P.; Prasad, A.K.; Tare, V.; Kafatos, M. Crop Yield Prediction Using Piecewise Linear Regression with a Break Point and Weather and Agricultural Parameters. U.S. Patent No. 7,702,597, 20 April 2010.

78. Prasad, A.K.; Singh, R.P.; Tare, V.; Kafatos, M. Use of Vegetation Index and Meteorological Parameters for the Prediction of Crop Yield in India. *Int. J. Remote Sens.* **2007**, *28*, 5207–5235. [CrossRef]
79. Stuart, B.H. *Infrared Spectroscopy: Fundamentals and Applications*; John Wiley & Sons: Hoboken, NJ, USA, 2004; ISBN 978-0-470-01113-3.
80. Pavia, D.L.; Lampman, G.M.; Kriz, G.S.; Vyvyan, J.A. *Introduction to Spectroscopy*, 5th ed.; Cengage Learning: Stamford, CT, USA, 2014; ISBN 978-1-305-17782-6.
81. Preety, K.; Prasad, A.K.; Varma, A.K.; El-Askary, H. Accuracy Assessment, Comparative Performance, and Enhancement of Public Domain Digital Elevation Models (ASTER 30 m, SRTM 30 m, CARTOSAT 30 m, SRTM 90 m, MERIT 90 m, and TanDEM-X 90 m) Using DGPS. *Remote Sens.* **2022**, *14*, 1334. [CrossRef]